Journal of Solid State Chemistry 182 (2009) 381–388

Contents lists available at ScienceDirect

Journal of Solid State Chemistry

journal homepage: www.elsevier.com/locate/jssc

N,*N*′-bis(salicylidene)propane-1,2-diamine lanthanide(III) coordination polymers: Synthesis, crystal structure and luminescence properties

Wen-Bin Sun, Peng-Fei Yan, Guang-Ming Li *, Hui Xu, Ju-Wen Zhang

Key Laboratory of Heilongjiang Province and Education Department of Heilongjiang Province, School of Chemistry and Materials Science, Heilongjiang University, No. 74, Xuefu Road, Nangang District, Harbin 150080, PR China

ARTICLE INFO

Article history:
Received 4 September 2008
Received in revised form
25 October 2008
Accepted 9 November 2008
Available online 21 November 2008

Keywords:
N, *N*′-bis(salicylidene)propane-12-diamine
Lanthanide
Structure
Luminescence

ABSTRACT

Reaction of $Ln(NO_3)_3 \cdot 6H_2O$ with H_2L [H_2L = *N*,*N*′-bis(salicylidene)propane-1,2-diamine] gives rise to five new coordination polymers, *viz.* $[Pr(H_2L)(NO_3)_3(MeOH)]_n$ (**1**) and $[Ln(H_2L)_{1.5}(NO_3)_3]_n$ [*Ln* = La (**2**), Eu (**3**), Sm (**4**) and Gd (**5**)]. Crystal structural analysis reveals that H_2L effectively functions as a bridging ligand forming one-dimensional (1D) chain and two-dimensional (2D) open-framework polymers. Solid-state fluorescence spectra of **3** and **4** exhibit typical red fluorescence of Eu(III) and Sm(III) ions at room temperature while **2** emits blue fluorescence of ligand H_2L. The lowest triplet level of ligand H_2L was calculated on the basis of the phosphorescence spectrum of **5.** The energy transfer mechanisms in the lanthanide polymers were described and discussed.

1. Introduction

Self-assembled lanthanide coordination polymers have recently attracted much attention because of their potential use in luminescence devices [1–4]. For the lanthanide ions, the *f*–*f* transitions are parity forbidden and the absorption coefficients are often very low. The photophysical properties of these ions depend markedly on their environments. To tune efficient emissions of lanthanide ions, a variety of multidentate organic ligands are employed in transferring absorbed energy efficiently to the lanthanide ions [5–8]. Salen-type ligands, as important multidentate acyclic ligands, have played essential role in tuning bioactivity and magnetic performance of organic lanthanide complexes [9–13]. However, their applications in moderating luminescence properties of lanthanide ions are seldom documented due to the difficulty in controlling the coordination environments of lanthanide(III) ions which display high and variable coordination numbers with little stereochemical preferences [6,14–16]. In addition, structurally characterized salen-type mononuclear lanthanide complexes are rare so far as to the diverse coordination mode of the numerous salen-type ligands [5,6,16–21]. E.g., only a few *N*,*N*′-bis(salicylidene)propane-1,2-diamine Fe(III) and V(IV, V) coordination complexes have been reported [22,23]. But, its mononuclear lanthanide complexes are unknown. Our recent studies have focused on the use of a variety of salen-type ligands to stabilize *Ln*(III) centers that provide the 'antenna' for lanthanide luminescence [24–26]. As part of our continuing studies focused on the assembly of these salen-type lanthanide systems we describe here the syntheses, structures and photophysical properties of five new salen-type lanthanide polymers.

2. Experimental

2.1. General

All operations were performed in an open atmosphere. *N*,*N*′-bis(salicylidene)propane-1,2-diamine (H_2L) was prepared according to the literature methods [27]. $Ln(NO_3)_3 \cdot 6H_2O$ (*Ln* = La, Pr, Sm, Eu and Gd) were prepared by reactions of lanthanide oxide and nitric acid. Elemental (C, H and N) analyses were performed on a Perkin-Elmer 2400 analyzer. IR spectra were determined on a Perkin-Elmer 60000 spectrophotometer. Thermal analyses were conducted on a Perkin Elmer DTA-1700 with a heating rate of $10\,^{\circ}C\,min^{-1}$. UV spectra were recorded in methanol at room temperature on a Shimadzu UV2240 spectrophotometer. Fluorescence spectra were taken on a Perkin-Elmer LS-55 fluorescence photometer at room temperature. Phosphorescence spectra were recorded on SPEX 1934D phosphorescence spectrometer at 77 K. Powder X-ray diffraction (PXRD) data were recorded on a Rigaku D/Max-3B X-ray diffractometer with Cu*K*α as the radiation source ($\lambda = 0.15406$ nm) in the angular range $2\theta = 5$–50° at room temperature.

* Corresponding author. Fax: +86 451 86608042.
E-mail address: gmli@hlju.edu.cn (G.-M. Li).

0022-4596/$ - see front matter © 2008 Elsevier Inc. All rights reserved.
doi:10.1016/j.jssc.2008.11.016

2.2. Preparation of polymers 1−5

Complexes **1–5** were prepared by similar procedures. To a MeOH solution (10 mL) of H_2L (0.086 g, 0.25 mmol) was slowly added a MeOH solution (10 mL) of [$Pr(NO_3)_3 \cdot 6H_2O$] (0.1087 g, 0.25 mmol) at ambient temperature. A yellow precipitate formed immediately. After stirring for 5 h, yellow solid was collected by filtration and washed with MeOH. Single crystals suitable for X-ray determination were obtained by slow diffusion of diethylether into a methanol solution of the powder sample over one week.

$[Pr(H_2L)(NO_3)_3(MeOH)]_n$ (**1**) yield: 0.12 g (85%). Elementary anal. calcd. for $C_{37}H_{49}N_{10}O_{25}Pr_2$ (1120.01): C, 46.11; H, 5.67; N, 12.51. Found: C, 46.01; H, 5.56; N, 12.21%. IR (KBr pellet, cm^{-1}): 3634 (m, ν(NH)), 3434 (m, ν(OH)), 1642 (vs, ν(C═N)), 1283 (vs, (C_{ph}–O) and/or ν_1 (NO_3^{-1})), 1481 (ν_4), 1022 (ν_2), 816 (ν_6), (bidentate chelating NO_3^{-1} group). λ_{max}/nm (ε_{max}/$dm^3\,mol^{-1}\,cm^{-1}$) (methanol), 211 (35621); 242 (15940); 256 (14408); 321(4986).

$[La(H_2L)_{1.5}(NO_3)_3]_n$ (**2**) yield: 0.1632 g (85%). Elementary anal. calcd. for $C_{51}H_{48}La_2N_{12}O_{24}$ (1490.88): C, 41.09; H, 3.25; N, 11.27. Found: C, 40.89; H, 3.10; N, 11.01%. IR (KBr pellet, cm^{-1}): 3409 (m, ν(NH)), 1644 (vs, ν(C═N)), 1277 (vs, (C_{ph}–O) and/or ν_1 (NO_3^{-1})), 1481 (ν_4), 1025 (ν_2), 816 (ν_6), (bidentate chelating NO_3^{-1} group). λ_{max}/nm (ε_{max}/$dm^3\,mol^{-1}\,cm^{-1}$) (methanol), 212 (32975); 254 (11871); 319 (3983); 377 (867).

$[Eu(H_2L)_{1.5}(NO_3)_3]_n$ (**3**) yield: 0.1623 g (83%). Elementary anal. calcd. for $C_{51}H_{51}Eu_2N_{12}O_{24}$ (1519.94): C, 40.30; H, 3.38; N, 11.06. Found: C, 40.25; H, 3.29; N, 10.95%. IR (KBr pellet, cm^{-1}): 3435 (m, ν(NH)), 1646 (vs, ν(C═N)), 1280 (vs, (C_{ph}–O) and/or ν_1 (NO_3^{-1})), 1480 (ν_4), 1027 (ν_2), 815 (ν_6), (bidentate chelating NO_3^{-1} group). λ_{max}/nm (ε_{max}/$dm^3\,mol^{-1}\,cm^{-1}$) (methanol), 211 (37782); 241 (17606); 256 (14950); 323 (4998).

$[Sm(H_2L)_{1.5}(NO_3)_3]_n$ (**4**) yield: 0.1662 g (85%). Elementary anal. calcd. for $C_{51}H_{51}Sm_2N_{12}O_{24}$ (1516.74): C, 40.39; H, 3.39; N, 11.08. Found: C, 40.45; H, 3.42; N, 11.13%. IR (KBr pellet, cm^{-1}): 3434 (m, ν(NH)), 1644 (vs, ν(C═N)), 1280 (vs, (C_{ph}–O) and/or ν_1 (NO_3^{-1})), 1478 (ν_4), 1025 (ν_2), 812 (ν_6), (bidentate chelating NO_3^{-1} group). λ_{max}/nm (ε_{max}/$dm^3\,mol^{-1}\,cm^{-1}$) (methanol), 211 (34887); 241 (22571); 256 (13553); 328 (4116).

$[Gd(H_2L)_{1.5}(NO_3)_3]_n$ (**5**) yield: 0.1643 g (84%). Elementary anal. calcd. for $C_{51}H_{51}Gd_2N_{12}O_{24}$ (1530.52): C, 40.02; H, 3.36; N, 10.98. Found: C, 40.10; H, 3.40; N, 10.90%. IR (KBr pellet, cm^{-1}): 3435 (m, ν(NH)), 1643 (vs, ν(C═N)), 1280 (vs, (C_{ph}–O) and/or ν_1 (NO_3^{-1})), 1479 (ν_4), 1026 (ν_2), 817 (ν_6), (bidentate chelating NO_3^{-1} group). λ_{max}/nm (ε_{max}/$dm^3\,mol^{-1}\,cm^{-1}$) (methanol), 211 (34356); 242 (21256); 256 (13106); 324 (4421).

2.3. X-ray crystallographic analysis

Diffraction intensity data for single crystals of complexes **1–3** were collected on a Rigaku R-AXIS RAPID imaging-plate X-ray diffractometer at 293 K. The structures were solved by the direct method and refined by the full-matrix least squares on F^2 using the SHELXTL-97 software package [28]. All non-hydrogen atoms were refined anisotropically. The C atoms of the diaminopropane link are disordered over two positions with site occupancy factors of ca. 0.7 and 0.3. Crystallographic data and important refinement parameters for **1–3** are summarized in Table 1.

3. Results and discussion

3.1. Preparation

Reactions of the ligand H_2L with $Ln(NO_3)_3 \cdot 6H_2O$ in a molar ratio of 1:1 were carried out in methanol at ambient temperature. Single crystals suitable for X-ray analysis were obtained by slow diffusion of diethylether into a methanol solution of the powder sample. As a result, two types of coordination polymers, $[Pr(H_2L)(NO_3)_3(MeOH)]_n$ and $[Ln(H_2L)_{1.5}(NO_3)_3]_n$ (Ln = La, Sm, Eu and Gd) (Scheme 1) were isolated. All the complexes **1–5** show no clear melting point before decomposing at ca. 260 °C.

3.2. IR spectroscopy

The infrared spectra of **1–5** are similar (Table 2), taking **1** as an example, the broad band for the O–H stretching vibration

Table 1
Crystallographic data for **1–3**.

Crystal data	1	2	3
Empirical formula	$C_{37}H_{49}N_{10}O_{25}Pr_2$	$C_{51}H_{48}La_2N_{12}O_{24}$	$C_{51}H_{51}Eu_2N_{12}O_{24}$
Formula weight	1315.68	1490.88	1519.96
Temperature (K)	291 (2)	293 (2)	293 (2)
Wavelength (Å)	0.71073	0.71073	0.71073
Crystal system space group	Monoclinic, $P2_1/c$	Trigonal R	Hexagonal $Pc1$
a (Å)	9.8701 (4)	16.5614 (6)	15.8346 (6)
b (Å)	16.0793 (7)	16.5614 (6)	15.8346 (6)
c (Å)	32.5235 (6)	51.574 (4)	17.5247 (7)
α (°)	90	90	90
β (°)	91.3800 (10)	90	90
γ (°)	90	120	120
V (Å^3)	5160.1 (4)	12250.6 (7)	3805.2 (4)
Z	4	6	2
Calculated density (Mg/m^3)	1.694	1.217	1.327
Absorption coefficient (mm^{-1})	1.958	1.099	1.705
Crystal size (mm)	0.20 × 0.11 × 0.09	0.30 × 0.30 × 0.24	0.23 × 0.18 × 0.16
Reflections collected	36951	22010	18598
Independent reflections	12761 [R(int) = 0.0484]	4816 [R(int) = 0.0357]	2189 [R(int) = 0.0295]
Completeness to theta = 25° (%)	99.6	99.9	97.7
Max. and min. transmission	0.8434 and 0.6954	0.7784 and 0.7340	0.7721 and 0.6952
Data/restraints/parameters	12761/7/693	4816/20/269	2189/13/140
Goodness-of-fit on F^2	1.001	1.256	1.156
Final R indices [$I>2\sigma(I)$]	$R1 = 0.0424$ w$R2 = 0.0768$	$R1 = 0.0685$ w$R2 = 0.1589$	$R1 = 0.0612$ w$R2 = 0.1535$

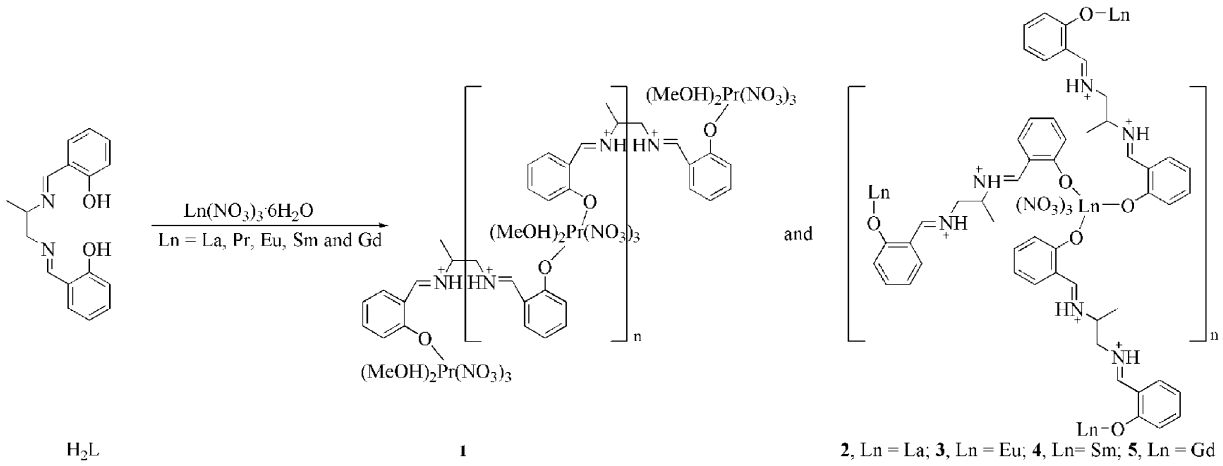

Scheme 1. Synthesis of polymers **1–5**.

Table 2
Infrared data for H_2L and polymers **1–5**.

Compounds	ν (cm^{-1})			
	O(N)–H	C=N	C–O	NO_3^{-1} (ν_4, ν_1, ν_2, ν_6)
H_2L	2837[a]	1628	1253	
1(Pr)	3634[a], 3434[b]	1642	1283	1481, 1283, 1022, 816
2(La)	3433[b]	1644	1277	1481, 1277, 1025, 816
3(Eu)	3435[b]	1646	1280	1480, 1280, 1027, 815
4(Sm)	3434[b]	1644	1280	1478, 1280, 1025, 812
5(Gd)	3435[b]	1643	1280	1479, 1280, 1026, 817

[a] The O–H vibration.
[b] The N–H vibration in $C=N^+$–H.

of ligand at ca. 2880 cm^{-1} (on which the CH modes are superimposed) is replaced by a band at ca. 3434 cm^{-1}, due to the N–H vibration in $C=N^+$–H. This band indicates that this hydrogen atom is still involving in the intramolecular H-bonding with the phenolic oxygen atom. It is consistent to that for the lanthanide complexes of zwitterionic Schiff-base ligand [29,30]. In addition, the complex **1** showed an O–H stretching frequency around 3634 cm^{-1} deriving from the coordinated MeOH molecule which was not found in complexes **2–5**. The similar vibration was found in the 1D polymeric complex $[La(H_2salen)(NO_3)_3(MeOH)_2]_n$ [21]. Coordination of the phenolic oxygen was also indicated by a significant increase in the C–O stretching frequency ($\Delta\nu\sim25$ cm^{-1}). Additionally, the C=N stretching vibration in ligand shifted to higher wavenumber by 14–18 cm^{-1} to about 1646 cm^{-1} after complexation. Four bands in the IR spectra of the complexes **1–5** near 1481(ν_4), 1283(ν_1), 1022(ν_2) and 816(ν_6) cm^{-1} can be assigned to vibrations of the coordinated nitrate group. The difference between the ν_4 and the ν_1 peak positions is ca. 200 cm^{-1}, which is typical for a η^2-chelation of the nitrate groups (monodentate nitrate groups display a much smaller splitting) [29,30].

3.3. Crystal structure analysis

X-ray crystallographic analysis reveals that **1** crystallizes in the monoclinic $P2_1/c$ space group. The unit cell contains one $[Pr(H_2L)(NO_3)_3]$ unit with two moles of crystalline methanol. Complex **1** loses approximately 5.1% in weight when heated to 130.7 °C. It suggests the presence of two moles of crystalline methanol in the empirical molar formula in the crystals. An infinite 1D chain structure results from the bridging ligand (H_2L) between each two Pr(III) ions through two Pr–O(phenolic) bonds (Fig. 1a). Each Pr(III) ion, adopting a distorted hexadecahedron geometry, is 10-coordinated with two phenolic oxygen atoms from different ligands, two methanol oxygen atoms and three bidentate nitrate oxygen atoms, while the nitrogen atoms of imine remain uncoordinated. Fig. 1b shows the packing view of **1**, there were two parallel polymeric chains extending along the *a* axis, where the adjacent chains are connected by O(12)–H(23)···O(23) (2.775(4) Å) interactions. The structure of **1** is identical to the 1D polymeric chain complex $[Ln(H_2salen)(NO_3)_3(CH_3OH)_2]_n$ (Ln = La and Pr) [21,25]. The distances of Pr–O(methanolic) bonds are 2.538(3) and 2.570(3) Å, respectively. The average bond length of Pr–O(nitrate) is 2.642 Å, which is slightly larger than that of 2D polymer $[Pr(H_2salen)_{1.5}(NO_3)_3]_n$ (2.593 Å). The shorter Pr–O bonds involving the deprotonated phenol oxygen atoms are 2.360(3) and 2.372(2) Å, respectively. It is close to that observed in our recently reported complexes $[Pr(H_2salen)(NO_3)_3(CH_3OH)_2]_n$ and $[Pr(H_2salen)_{1.5}(NO_3)_3]_n$ [25] (Table 3). However, the O(1)–Pr–O(2A) angle is 157.3(5)° which is markedly larger than that of complex $[Pr(H_2salen)(NO_3)_3(CH_3OH)_2]_n$ (71.2(1)°) and $[Pr(H_2salen)_{1.5}(NO_3)_3]_n$ (93.9(1)°) (Table 3). This is close to the angle of O(phenolic)–La–O(phenolic) in 1D chain complex $[La(H_2salen)(NO_3)_3(CH_3OH)_2]_n$ (144.5(2)°) [21]. Thus, the 1D chains bridged by ligand H_2L are nearly in a linear configuration. Furthermore, the hydrogen atoms located on the two nitrogen atoms are involved in intramolecular hydrogen bonding with the deprotonated phenol oxygen atoms, which indicated that a proton migration occurs in the complexation reactions.

X-ray crystallographic analyses reveal that the structures of **2** and **3** are similar whereas they crystallize in trigonal $R\bar{3}$ and hexagonal $P\bar{3}c1$ space groups, respectively. The experimental and simulated PXRD spectra of **3–5** are shown in supplementary materials (Fig. S1). The main diffraction peaks and the patterns of the main peaks for **3–5** are essentially similar that indicates they are isomorphic. A representative structure of **2** including the atomic numbering scheme is described in Fig. 2. In **2**, the unit cell contains $[La(H_2L)_{1.5}(NO_3)_3]$ without any solvent molecules. Each La(III) ion, adopting a nine-coordinated tricapped trigonal prismatic geometry (Fig. 2a), is ligated by three bidentate nitrate and three independent ligands that utilize only one hydroxyl oxygen atom. The distorted trigonal prism is composed of O(1), O(1A), O(1B) and O(4), O(4A) O(4B) atoms. The O(2), O(2A) and O(2B) atoms are at the vertices of each square pyramid and the two triangular faces is parallel (Fig. 2a). Each ligand acts as a bidentate linker bridging between two La(III) ions through the two hydroxy

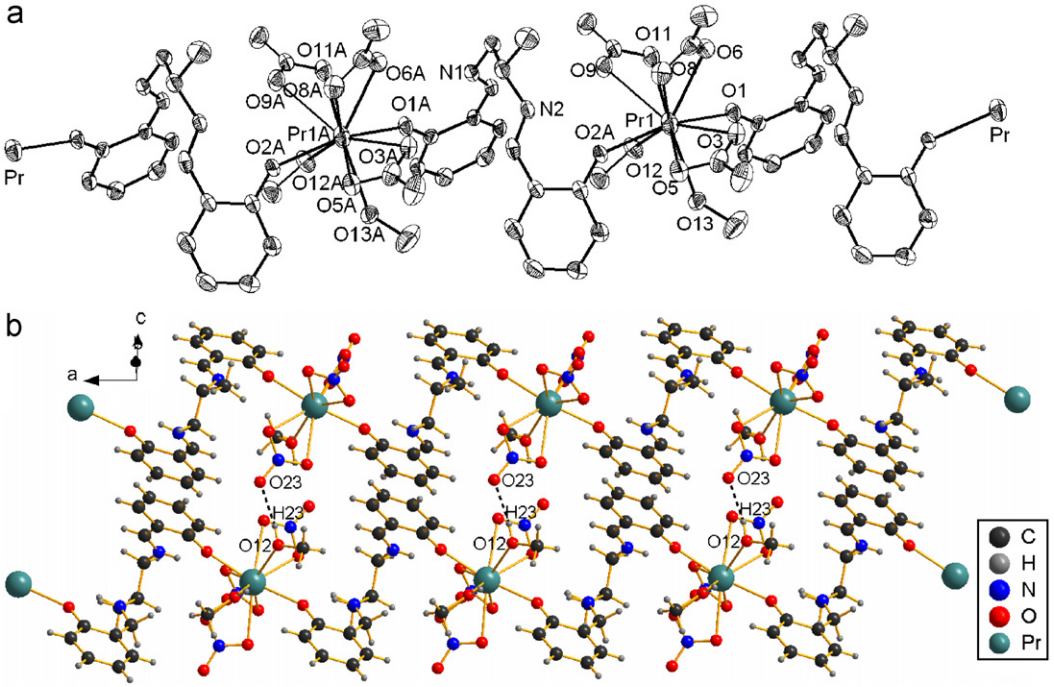

Fig. 1. (a) Ortep plot of the crystal structure for complex **1** (30% thermal ellipsoids and hydrogen atoms removed for clarity). Selected bond lengths (Å) and bond angles (°): Pr(1)–O(1) 2.360(3), Pr(1)–O(2A) 2.372(2), Pr(1)–O(3) 2.558(3), Pr(1)–O(5) 2.640(3), Pr(1)–O(6) 2.587(3), Pr(1)–O(8) 2.672(3), Pr(1)–O(9) 2.624(3), Pr(1)–O(11) 2.773(3), Pr(1)–O(12) 2.538(3), Pr(1)–O(13) 2.570(3), O(1)–Pr(1)–O(2A) 157.3(5). Hydrogen bond for **1** (Å and °) O(12)–H(23) 0.842(7), H(23)···O(23) 1.99(2), O(12)–H(23)···O(23) 155(5); (b) Packing drawing showing the polymeric chains, the chains are self-assembled through hydrogen bonds shown in dotted lines.

Table 3
Average bond lengths (Å) and bond angles (°) for H_2L-Pr (**1**) and H_2salen-Pr.

Bond lengths /angles	H_2L-Pr (**1**)	H_2salen-Pr[a]	H_2salen-Pr[b]
Pr–O (phenolic)	2.366	2.377	2.360
Pr–O (nitrate)	2.642	2.645	2.593
Pr–O (methanolic)	2.554	2.542	
O (phenolic)–Pr–O (phenolic)	157.3	71.2	93.9

[a] Complex $[Pr(H_2salen)(NO_3)_3(MeOH)_2]_n$.
[b] Complex $[Pr(H_2salen)_{1.5}(NO_3)_3]$ in Ref. [25].

oxygen atoms (Fig. 2a). The La–La distance through the bridge is 9.8782(4) Å and the Eu–Eu distance is 9.500(4) Å. In addition, six La(III) ions are formed in a circular fashion through the bondings of lanthanide and deprotonated ligand (Fig. 2b). Finally, the La(III) ions connected by the ligands create a 2D layered structure containing an hexagonal pattern. The La(III) ions are not completely coplanar, but form corrugated planes. This structural motif is repeated along the *z* axis (Fig. 2c), forming spacious channels. The formation of this honeycomb pattern resembles those found in $[Eu(Hida)_3]_xH_2O$ (H_2ida = iminodiacetic acid) [31] and $[Eu_2L^1_3(DMSO)_2(MeOH)_2]\cdots 2DMSO\cdots 3H_2O$ (L^1 = 4,4′-ethyne-1,2-diyldibenzoate) [32]. However, it is a rare example for complexes containing only a lanthanide ion and a salen-type ligand. The diameters of these channels (defined as the C–C distance of opposite H_2L ligands) are ca. 10.098 Å. They are almost the same as that of **3**, 10.009 Å. Surprisingly, the structure of **2** is different from other tetradentate salen-type lanthanum complexes $[La(H_2salen)(NO_3)_3(MeOH)_2]_n$ [21] and $[La_2L^2(NO_3)_6]_n$ (L^2 = N,N′-bis(salicylidene)-1,4-butanediamine) [16] in which they are 1D chain and 2D polymeric structure, respectively. Obviously, the ligand and reaction condition may dominate the final structure of these coordination complexes and particularly their dimensionality [16,17].

The La–O bond distances, divided into three groups, are 2.410(4), 2.593(4) and 2.617(5) Å (Table 4). The three bond lengths of La–O(phenolic) are identical, being 2.410(4) Å, they are close to those observed in tetradentate salen-type complexes $[La(H_2salen)(NO_3)_3(MeOH)_2]_n$ (2.430 Å) [21] and $[La_2L^2(NO_3)_6]_n$ (2.460 Å) [16], where the La(III) was 10-coordinated. The average bond length of La–O(nitrate) is 2.605 Å, which is slightly shorter than that of $[La(H_2salen)(NO_3)_3(MeOH)_2]_n$ (2.672 Å) and $[La_2L^2(NO_3)_6]_n$ (2.680 Å). Relative structural parameters of tetradentate salen-type lanthanum complexes are gathered in Table 5. The O–La–O angles are in the range of 48.53(5)–164.75(6)°. It is worth noting that the bond angles of O(phenolic)–La–O(phenolic), namely, O(1A)–La(1)–O(1B), O(1A)1–La(1)–O(1) and O(1B)–La(1)–O(1) are identical, being 92.72(4)°, which is almost a right angle (90°). The bond angles O(1A)–La(1)–O(4), O(1B)–La(1)–O(4A) and O(1)–La(1)–O(4B) are 120.35(4)° and the angles of O(1B)–Ln(1)–O(4B), O(1A)–Ln(1)–O(4A) and O(1)–Ln(1)–O(4) are 145.41(5)°. Relevant structural parameters of **2** and **3** are gathered in Table 4.

3.4. Luminescent properties

All absorption spectra in methanol at room temperature exhibited similar bands between 256 and 328 nm. They can be assigned to π–π^* transitions of the ligand H_2L. The new absorption band at ca. 242 nm, which was absent both for the free ligand and $Ln(NO_3)_3$, was attributed to the electron transfer between the metal center and the coordinated ligand H_2L [21,26]. The solid-state fluorescence spectra of the complexes were measured at room temperature. In contrast to the weak luminescence of the free ligand, **2** exhibits one strong band centered at 490 nm exited at 340 nm in the solid state (Fig. 3a, Table 6). Since there are no 4*f* electrons and the energy level of excited states below the triplet levels of the ligand for La(III) ions, the energy absorbed by the

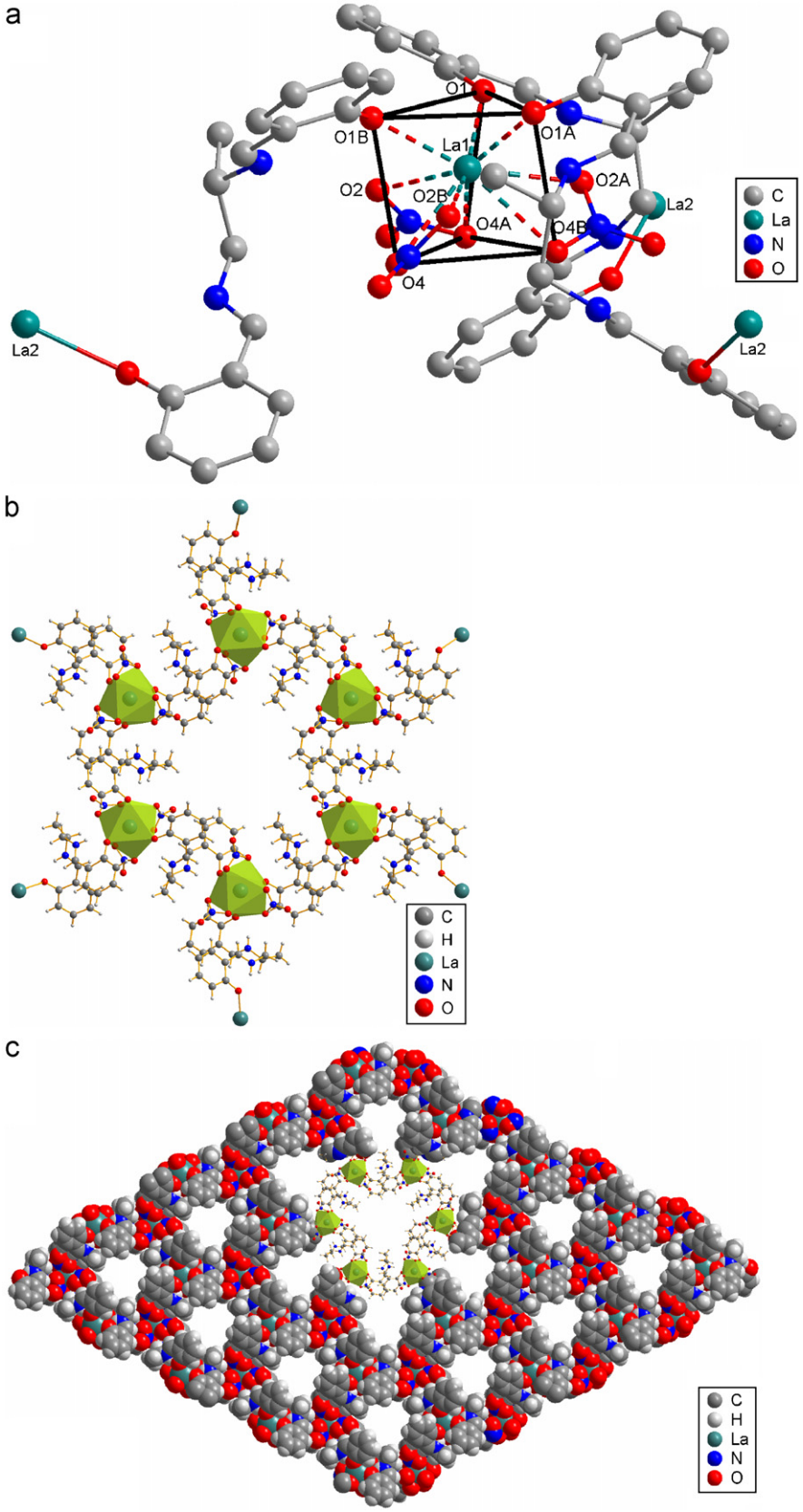

Fig. 2. (a) Perspective view of **2** (hydrogen atoms removed for clarity); (b) view of a H_2L bridged hexametal ring along the *c* axis for **2**; (c) space-filling and polyhedral view of the packing of layers along the *c* axis for **2**.

Table 4
Selected bond lengths (Å) and bond angle (°) for complexes **2** and **3**.

Bond lengths/angles	La(**2**)	Eu(**3**)
Ln(1)–O(1)/O(1A)/ O(1B)	2.410 (4)	2.297 (5)
Ln(1)–O(2)/O(2A)/ O(2B)	2.593 (4)	2.544 (5)
Ln(1)–O(4)/O(4A)/ O(4B)	2.617 (5)	2.522 (5)
O(1A)–Ln(1)–O(1B)/O(1A)1–Ln(1)–O(1)/O(1B)–Ln(1)–O(1)	92.72 (4)	92.06 (5)
O(1A)–Ln(1)–O(4)/O(1B)–Ln(1)–O(4A)/O(1)–Ln(1)–O(4B)	120.35 (4)	121.48 (4)
O(1B)–Ln(1)–O(4B)/O(1A)–Ln(1)–O(4A)/O(1)–Ln(1)–O(4)	145.41 (5)	145.88 (6)
Ln(2)–O(5)/O(5C)/O(5D)	2.396 (4)	
Ln(2)–O(8)/O(8C)/O(8D)	2.631 (5)	
Ln(2)–O(6)/O(6C)/O(6D)	2.643 (5)	
O(5)–Ln(2)–O(5C)/O(5)–Ln(2)–O(5D)/O(5C)–Ln(2)–O(5D)	96.79 (6)	
O(5C)–Ln(2)–O(8C)/O(5D)–Ln(2)–O(8D)/O(5)–Ln(2)–O(8)	119.00 (5)	
O(5C)–Ln(2)–O(8)/O(5D)–Ln(2)–O(8C)/O(5)–Ln(2)–O(8D)	144.14 (6)	

Symmetry operation: (A) $-y+1, x-y-1, z$; (B) $-x+y+2, -x+1, z$; (C) $-y+1, x-y, z$; (D) $-x+y+1, -x+1, z$ for **2**; (A) $-x+y+1, -x+1, z$; (B) $-y+1, x-y, z$ for **3**.

Table 5
Selected structural parameters for complexes $[La(H_2L)_{1.5}(NO_3)_3]_n$ (**2**), $[La(H_2salen)(NO_3)_3(MeOH)_2]_n$ and $[La_2L^2(NO_3)_6]_n$.

	$[La(H_2L)_{1.5}(NO_3)_3]_n$	$[La(H_2salen)(NO_3)_3(MeOH)_2]_n$	$[La_2L^2(NO_3)_6]_n$
Coordination numbers	9	10	10
Dimensionality	2D	1D	2D
La–O (phenolic) (Å)	2.410	2.430	2.460
La–O (nitrate) (Å)	2.605	2.672	2.680

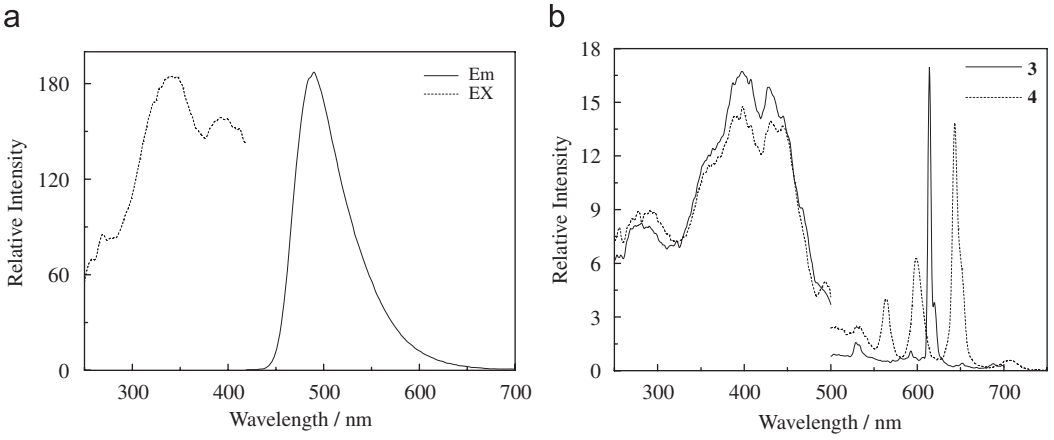

Fig. 3. Excitation and emission spectra of **2** (a), **3** and **4** (b) in the solid state.

Table 6
Fluorescent data for **2**, **3** and **4**.

Complexes	λ_{ex}(nm)	λ_{em}(nm)	Transition type
2 (La)	340	490	π–π^*
3 (Eu)	397	592, 614	$^5D_0 \rightarrow {}^7F_1$, $^5D_0 \rightarrow {}^7F_2$
4 (Sm)	399	564, 599, 644, 705	$^4G_{5/2} \rightarrow {}^6H_{5/2}$, $^4G_{5/2} \rightarrow {}^6H_{7/2}$, $^4G_{5/2} \rightarrow {}^6H_{9/2}$, $^4G_{5/2} \rightarrow {}^6H_{11/2}$

ligand H_2L cannot transfer to La(III) ions. The absorbed energy can only relax through its own lower energy levels. The intense blue fluorescence emission of **2** are attributed to the enhanced π–π^* electron transition of the ligand. Therefore, **2** emits the ligand-centered fluorescence. The half-band width of **2** is 62 nm. It is markedly narrower than those for complexes $La(PMIP)_3(TPPO)_2$ (PMIP = 1-phenyl-3-methyl-4-isobutyryl-5-pyrazoloneate, TPPO = triphenyl phosphine oxide) (116 nm) $La(PMIP)_3(Bipy)_2$ (Bipy = 2,2′-dipyridine) (110 nm) and $La(PMIP)_3(Phen)_2$ (Phen = 1,10-phenanthroline) (129 nm) [33]. The emitting bands of these complexes are centered at 435, 460 and 497 nm that emits blue and blue-green fluorescence, respectively. The half-band width of **2** is close to that of Schiff-base complexes $ZnBSO\cdots H_2O$ (68 nm) (H_2BSO = *N,N′*-bis(salicylidene)-3, 6-dioxa-1,8-diaminooctane) and BDPMB-Zn (BDPMB = 2,3-bis[(4-diethylamino-2-hydroxybenzylidene)amino]but-2-enedinitrile) (40 nm) [34,35]. On comparing with complexes Alq_3 and Gaq_3 (q = 8-hydroxyquinoline) [36,37] with ligand-centered fluorescence that are used as

electroluminescence or photoluminescence materials, the ligand-centered fluorescence for lanthanide complexes needs further exploring [33,38,39].

The emission spectrum of **3** mainly shows two narrow bands at 592 and 614 nm under the excitation at 397 nm (Fig. 3b). They are attributed to the characteristic emission $^5D_0 \rightarrow {}^7F_1$ and $^5D_0 \rightarrow {}^7F_2$ transition of Eu(III) ion, respectively. The $^5D_0 \rightarrow {}^7F_2$ transition is the induced electric dipole transition, which is greatly affected by the coordination environment. The $^5D_0 \rightarrow {}^7F_1$ transition (592 nm) is the magnetic dipole transition, which is much less sensitive to the environment [40–46]. The $^5D_0 \rightarrow {}^7F_2$ transition is clearly stronger than the $^5D_0 \rightarrow {}^7F_1$ transition, which indicates the absence of inversion symmetry at Eu(III) site [40–43]. This phenomena is consistent with the structure of **3**. X-ray diffraction analysis of **3** revealed that the ligands shield Eu(III) ions and there is no solvent molecule coordinate to Eu(III) ions. Thus, **3** displays comparatively strong red luminescence of Eu(III) ion.

The emission spectrum of **4** consists of four bands at 564, 599, 644 and 705 nm that are assigned to the characteristic transitions of $^4G_{5/2} \rightarrow {}^6H_J$ ($J = \frac{5}{2}, \frac{7}{2}, \frac{9}{2}$ and $\frac{11}{2}$) in Sm(III) ions (Fig. 3b). It is different from complex $Sm(DPAP)_3 \cdot 12H_2O$ (HDPAP = 6-dipheny-lamine carbonyl 2-pyridine carboxylic acid) [47] and our recently reported salen-type lanthanide complex $[Sm(H_2L^3)(NO_3)_3(MeOH)_2]_n$ (H_2L^3 = *N*,*N*′-bis(salicylidene)-1, 2-cyclohexanediamine) [26], in which the emission band around 600 nm originated from the transition of magnetic dipole ($^4G_{5/2} \rightarrow {}^6H_{7/2}$) is the strongest. It is similar to the complexes $[\{Sm(OBz)_3(MeO)_2\}_2]_n$ (HOBz = benzoic acid), $[Sm(TTA)_3 \cdots 2L^4]$ (TTA = 2-thenoyltrifluoroacetone, $L^4 = H_2O$, TPPO, PHA, DBSO and PTSO) [48,49] and tetradentate salen complex $[Sm(H_2salen)_{1.5}(NO_3)_3]_n$ [25], however, the emission band at 644 nm from the transition of electronic dipole ($^4G_{5/2} \rightarrow {}^6H_{9/2}$) is the strongest for **4**. This is attributed to the different symmetry of Sm(III) ions in the complex [47]. Noticeable, these luminescent colors of **2**, **3** and **4** can be easily visualized using a standard laboratory UV lamp ($\lambda_{ex} = 365$ nm, Fig. 4), indicating intense luminescence of the complexes.

3.5. Triplet state of the ligand and energy transfer

To demonstrate the energy transfer process, the phosphorescence spectrum of $[Gd(H_2L)_{1.5}(NO_3)_3]_n$ (**5**) was measured at 77 K in a mixed solution of ethanol and methanol ($v/v = 1:1$). The triplet state energy level (T_1) of H_2L is 19920 cm^{-1}, which was calculated from the shortest-wavelength phosphorescence band. The energy gaps between the triplet state of H_2L and the resonance energy level of *Ln*(III) (*Ln* = Sm, Eu) are calculated and shown in Table 7.

It is known that the intermolecular transfer efficiency has a close relationship to the energy gap between the lowest triplet energy level (T_1) of the ligand and the lowest excited state level of *Ln*(III) ion [1]. The gap $\Delta E(T_1 - Ln(III))$ should be intermediate. Too big or too small would decrease the efficiency of energy transfer [41,50,51]. It is established that $\Delta E(T_1 - {}^5D_4) = 2400 \pm 300\ cm^{-1}$ for the organic ligand at room temperature would more efficiently sensitize luminescence of Tb(III) ion. Whereas, $\Delta E(T_1 - {}^5D_1) > 4000\ cm^{-1}$ for Eu (III) complex or $\Delta E(T_1 - {}^5D_4) < 1500\ cm^{-1}$ for Tb(III) complex would much more reduce the fluorescence yield [1,50,51]. As can be noticed in Table 7, the lowest triplet state level of the ligand H_2L was higher by 2643 and 2020 cm^{-1} than the lowest excited state level of Eu(III) ($^5D_0$) and Sm(III) ($^4G_{5/2}$). Therefore, strong luminescences are observed for **3** and **4**. They are close to that of complexes [Eu-3PTFA] (3PTFA = 3-Phenanthoyltrifluoroacetone) (2523 cm^{-1}) [51], [Eu-2NTFA] (NTFA = 2-Naphthoyltrifluoroacetone) (2323 cm^{-1}) [51] and $Sm(DPAP)_3 \cdot 12H_2O$ (2778 cm^{-1}) [47]. However, the lowest triplet state energy of H_2L is lower than that of the lowest excited state level of Tb(III) and Dy(III) ions so that the characteristic emissions of Tb(III) and Dy(III) ions were not observed. It is obvious that a good organic ligand of lanthanide(III) ions should have proper triplet energy levels.

To describe the mechanism, a diagram describing the energy transfer is showed in Fig. 5. The sensitization pathway in luminescent complexes **3** and **4**, in general, consists of excitation of the ligand (H_2L) into their excited singlet states (S_1), subsequent intersystem crossing (ISC) of the ligands to their triplet states (T_1), and energy transfer (ET) from the triplet state to the $^5D_0$ and $^6H_{5/2}$ level of Eu(III) and Sm(III) ions, followed by internal conversion to the emitting $^7F_{j,j}$ and $^6H_{j,j}$ state. Consequently, **3** and **4** exhibit the characteristic red fluorescence of Eu(III) and Sm(III) ions when a transition to the ground state occurs.

4. Conclusions

Isolation of **1–5** indicates that *N*,*N*′-bis(salicylidene)propane-1,2-diamine is able to stabilize the lanthanide ions to form two types of lanthanide coordination polymers. The size and the character of the lanthanide ions may dominate the structure of coordination polymers in this paper. The solid-state fluorescent spectra suggest that *N*,*N*′-bis(salicylidene)propane-1,2-diamine

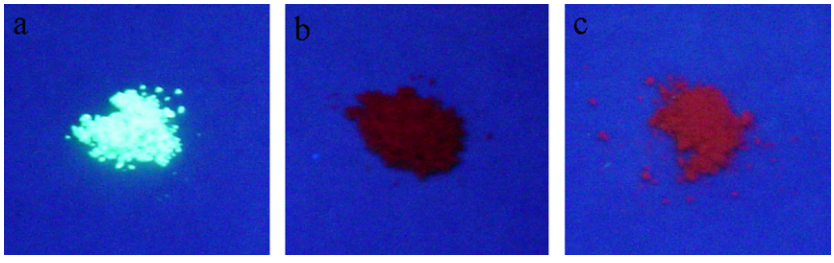

Fig. 4. Photograph of the solid powder samples **2** (a), **3** (b) and **4** (c) upon excitation by a standard laboratory UV lamp ($\lambda_{ex} = 365$ nm).

Table 7
The lowest triplet energy of Gd(III) complex with H_2L and the energy difference.

Lanthanide	The resonant level (cm^{-1})	Lowest triplet state energy (cm^{-1})	$\Delta E(T_1 - Ln(III))$ (cm^{-1})
Eu	17277	19920	2643
Sm	17900	19920	2020

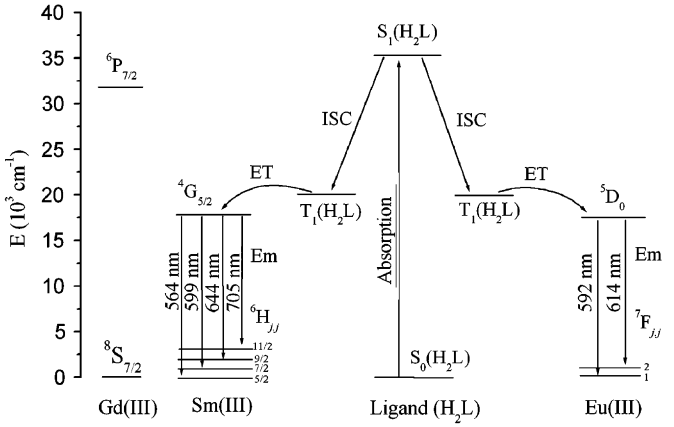

Fig. 5. Schematic energy level diagram and the energy transfer process.

plays an efficient ligand-to-metal energy transfer (antenna effect) that enhances the characteristic metal-centered fluorescence of Eu(III) and Sm(III) ions. The fluorescence of **3** and **4** are correlated to the gap of energy level between T_1 of ligand and the lowest excited state level of *Ln*(III) ion (*Ln* = Eu or Sm). These complexes with intense luminescence could be served as potential luminescence materials. This approach of incorporating salen-type ligand into lanthanide ions presents opportunities for the design of functional materials.

Supplementary materials

Crystallographic data for the structural analysis have been deposited with the Cambridge Crystallographic Center, CCDC Nos. 693971, 693970, 693969 for 1–3, respectively. Copies of this information may be obtained free of charge from The Director, CCDC, 12, Union Road, Cambridge, CB2, 1EZ, UK (fax: +44-1223-336-033; or e-mail: deposit@ccdc.cam.ac.uk or http://www.ccdc.ac.uk).

Acknowledgments

This work is financially supported by the National Natural Science Foundation of China (nos. 20672032 and 20572018), Key Laboratory of Heilongjiang Province and Education Department of Heilongjiang Province (nos. ZJG0504, JC200605, 1152GZD02, 2006FRFLXG031 and 11531284).

Appendix A. Supplementary material

Supplementary data associated with this article can be found in the online version at 10.1016/j.jssc.2008.11.016.

References

[1] H.J. Zhang, R.H. Gou, L. Yan, R.D. Yang, Spectrochim. Acta 66A (2007) 289–294.
[2] A. Edwards, C. Claude, I. Sokolik, T.Y. Chu, Y. Okamoto, R. Dorsinville, J. Appl. Phys. 82 (1997) 1841–1846.
[3] G.E. Buono-core, H. Li, B. Marciniak, Coord. Chem. Rev. 90 (1990) 55–87.
[4] V. Balzani, J.M. Lehn, J. van de Loosdrecht, A. Mecati, N. Sabbatini, J.M. Lehn, R. Ziessel, Angew. Chem. Int. Ed. Engl. 30 (1991) 190–191.
[5] X.P. Yang, R.A. Jones, W.K. Wong, J. Chem. Soc. Dalton Trans. (2008) 1676–1678.
[6] W. Dou, J.N. Yao, W.S. Liu, Y.W. Wang, J.R. Zheng, D.Q. Wang, Inorg. Chem. Commun. 10 (2007) 105–108.
[7] P. Guerriero, S. Tamburini, P.A. Vigato, Coord. Chem. Rev. 139 (1995) 17–243.
[8] N. Sabbatini, M. Guardigli, J.M. Lehn, Coord. Chem. Rev. 123 (1993) 201–228.
[9] J.C.G. Bünzli, C. Piguet, Chem. Rev. 102 (2002) 1897–1928.
[10] A. Huignard, T. Gacoin, J.P. Boilot, Chem. Mater. 12 (2000) 1090–1094.
[11] R.M. Supkowski, J.P. Bolender, W.D. Smith, Coord. Chem. Rev. 185/186 (1999) 307–319.
[12] P.H. Smith, J.R. Brainard, D.E. Morris, G.D. Jarvinen, R.R. Ryan, J. Am. Chem. Soc. 111 (1989) 7437–7443.
[13] P. Zanello, S. Tamburini, P.A. Vigato, G.A. Mazzocchin, Coord. Chem. Rev. 77 (1987) 165–273.
[14] C. Galoup, C. Dicord, B. Cathala, Helv. Chem. Acta 82 (1999) 543–560.
[15] Y.X. Ceng, M.Q. Jin, H.W. Shu, Progress in Coordination Chemistry, 251, vol. 8, Higher Education Press, Beijing, 2000, p. 17.
[16] W. Radecka-Paryzek, I. Pospieszna-Markiewicz, M. Kubicki, Inorg. Chim. Acta 360 (2007) 488–496.
[17] J. Chakraborty, G. Pilet, M.S. El. Fallah, J. Ribas, S. Mitra, Inorg. Chem. Commun. 10 (2007) 489–493.
[18] X.P. Yang, R.A. Jones, J. Am. Chem. Soc. 127 (2005) 7686–7687.
[19] M.T. Kaczmarek, I. Pospieszna-Markiewicz, M. Kubicki, W. Radecka-Paryzek, Inorg. Chem. Commun. 7 (2004) 1247–1249.
[20] J.P. Costes, F. Dahan, F. Nicodème, Inorg. Chem. 42 (2003) 6556–6563.
[21] W.H. Xie, M.J. Heeg, P.G. Wang, Inorg. Chem. 38 (1999) 2541–2543.
[22] N.F. Choudhary, N.G. Connelly, P.B. Hitchcock, G.J. Leigh, J. Chem. Soc. Dalton Trans. (1999) 4437–4446.
[23] Z.L. You, L.L. Tang, H.L. Zhu, Acta Cryst. E 61 (2005) m36–m38.
[24] T. Gao, P.F. Yan, G.M. Li, G.F. Hou, J.S. Gao, Inorg. Chim. Acta 361 (2008) 2051–2058.
[25] T. Gao, P.F. Yan, G.M. Li, G.F. Hou, J.S. Gao, Polyhedron 26 (2007) 5382–5388.
[26] P.F. Yan, W.B. Sun, G.M. Li, C.H. Nie, T. Gao, Z.Y. Yue, J. Coord. Chem. 60 (2007) 1973–1982.
[27] K. Ambroziak, Z. Rozwadowski, T. Dziembowska, B. Bieg, J. Mol. Struct. 615 (2002) 109–120.
[28] G.M. Sheldrick, SHELXS 97, Program for the Solution of Crystal Structures, University of Göttingen, Germany, 1997.
[29] K. Binnemans, Y.G. Galyametdinov, R.V. Deun, D.W. Bruce, S.R. Collinson, A.P. Olishchuk, I. Bikchantaev, W. Haase, A.V. Prosvirin, L. Tinchurina, I. Litvinov, A. Gubajdullin, A. Rakhmatullin, K. Uytterhoeven, L.V. Meervelt, J. Am. Chem. Soc. 122 (2000) 4335–4344.
[30] J.P. Costes, J.P. Laussac, F. Nicodème, J. Chem. Soc. Dalton Trans. (2002) 2731–2736.
[31] C. Kremer, P. Morales, J. Torres, J. Castiglioni, J. González-Platas, M. Hummert, H. Schumann, S. Domínguez, Inorg. Chem. Commun. 11 (2008) 862–864.
[32] B.T.N. Pham, L.M. Lund, D.T. Song, Inorg. Chem. 47 (2008) 6329–6335.
[33] D.Q. Gao, M. Guan, H. Xin, Z.Q. Bian, C.H. Huang, J. Rare Earth 22 (2004) 206–209.
[34] T.Z. Yu, W.M. Su, W.L. Li, Z.R. Hong, R.N. Hua, M.T. Li, B. Chu, B. Li, Z.Q. Zhang, Z.Z. Hu, Inorg. Chim. Acta 359 (2006) 2246–2251.
[35] P.F. Wang, Z.R. Hong, Z.Y. Xie, S.W. Tong, O.Y. Wong, C.S. Lee, N. Wong, L.S. Hung, S. Lee, Chem. Commun. (2003) 1664–1665.
[36] C.W. Tang, S.A. Van Styke, Appl. Phys. Lett. 51 (1987) 913–915.
[37] J. Qiao, L.D. Wang, L. Duan, Y. Li, D.Q. Zhang, Y. Qiu, Inorg. Chem. 43 (2004) 5096–5102.
[38] H. Xin, M. Shi, F.Y. Li, M. Guan, D.Q. Gao, C.H. Huang, K. Ibrahimc, F.Q. Liu, New J. Chem. 27 (2003) 1485–1489.
[39] C.H. Huang, F.Y. Li, W. Huang, Introduction to Organic Light-Emitting Materials and Devices, Fudan University Press, Shanghai, 2005, p. 435.
[40] Y. Liu, S.X. Liu, R.G. Cao, H.M. Ji, S.W. Zhang, Y.H. Ren, J. Solid State Chem. 181 (2008) 2237–2242.
[41] Y. Huang, B. Yan, M. Shao, Z.X. Chen, J. Mol. Struct. 871 (2007) 59–66.
[42] C.D. Wu, Z.Y. Liu, J. Solid State Chem. 179 (2006) 3500–3504.
[43] Y. Tang, K.Z. Tang, J. Zhang, C.Y. Su, W.S. Liu, M.Y. Tan, Inorg. Chem. Commun. 8 (2005) 1018–1021.
[44] D.T. de Lill, N.S. Gunning, C.L. Cahill, Inorg. Chem. 44 (2005) 258–266.
[45] B.L. An, M.L. Gong, K.W. Cheah, J.M. Zhang, K.F. Li, Chem. Phys. Lett. 385 (2004) 345–350.
[46] Y.B. Wang, X.J. Zheng, W.J. Zhuang, L.P. Jin, Eur. J. Inorg. Chem. (2003) 1355–1360.
[47] B.L. An, M.L. Gong, M.X. Lia, J.M. Zhang, J. Mol. Struct. 687 (2004) 1–6.
[48] U.P. Singh, R. Kumar, S. Upreti, J. Mol. Struct. 831 (2007) 97–105.
[49] H.F. Brito, O.L. Malta, M.C.F.C. Felinto, E.E.S. Teotonio, J.F.S. Menezes, C.F.B. Silva, C.S. Tomiyama, C.A.A. Carvalho, J. Alloys Compd. 344 (2002) 293–297.
[50] Y.S. Yang, M.L. Gong, Y.Y. Li, H.Y. Lei, S.L. Wu, J. Alloys Compd. 207/208 (1994) 112–114.
[51] S. Sato, M. Wada, Bull. Chem. Soc. Jpn. 43 (1970) 1955–1962.